Hard electron energy distribution in the relativistic shocks of gamma-ray burst afterglows

L. Resmi, D. Bhattacharya

Mon. Not. R. Astron. Soc. **388,** 144–158 (2008) doi:10.1111/j.1365-2966.2008.13298.x

Hard electron energy distribution in the relativistic shocks of gamma-ray burst afterglows

L. Resmi[1,2,3]★ and D. Bhattacharya[3,4]★

[1]*Institut d'Astrophysique de Paris, Paris 75014, France*
[2]*Indian Institute of Science, Bangalore 560012, India*
[3]*Raman Research Institute, Bangalore 560080, India*
[4]*Inter-University Centre for Astronomy & Astrophysics, Pune 411007, India*

Accepted 2008 April 6. Received 2008 April 5; in original form 2007 December 5

ABSTRACT

Particle acceleration in relativistic shocks is not a very well understood subject. Owing to that difficulty, radiation spectra from relativistic shocks, such as those in gamma-ray burst (GRB) afterglows, have been often modelled by making assumptions about the underlying electron distribution. One such assumption is a relatively soft distribution of the particle energy, which need not be true always, as is obvious from observations of several GRB afterglows. In this paper, we describe modifications to the afterglow standard model to accommodate energy spectra which are 'hard'. We calculate the overall evolution of the synchrotron and Compton flux arising from such a distribution. We also model two afterglows, GRB010222 and GRB020813, under this assumption and estimate the physical parameters.

Key words: acceleration of particles – gamma rays: bursts.

1 INTRODUCTION

Relativistic particles accelerated by shocks occupy a predominant place in astrophysical systems. These particles emit synchrotron and Compton radiation, which can be observed from radio to gamma-ray bands. Gamma-ray bursts (GRBs), their afterglows, supernova remnants, active galactic nuclei (AGN) and pulsar wind nebulae (PWNe) are some of the most important and intriguing candidates which house shock accelerated electron population.

The details of these electron populations and hence the details of the acceleration process are inferred from studying the emitted synchrotron and Compton radiation. The accelerated particles are often found to be distributed non-thermally, as a power law in energy characterized by an index p:

$$N(\gamma_e) = K_e \gamma_e^{-p}, (\gamma_m \leqslant \gamma_e < \gamma_u), \quad (1)$$

where $N(\gamma)\,\mathrm{d}\gamma$ is the number density of electrons in the energy interval $\gamma m_e c^2$ and $(\gamma + \mathrm{d}\gamma)m_e c^2$.

This non-thermal power law is a natural outcome of the Fermi process (Fermi 1949), a standard framework to describe shock acceleration. Several analytical and numerical investigations have been made (Achterberg et al. 2001; Ostrowski & Bednarz 2002; Ellison & Double 2004; Keshet 2006; Nishikawa et al. 2006) especially for the diffusive shock acceleration (DSA) mechanism, a variant of the Fermi first-order process, which is expected to operate in collisionless shocks. Most of the theoretical and numerical studies produce a 'single soft' distribution of the accelerated particles, where the index p is greater than two.

Though there are many observations supporting this prediction, a non-negligible fraction seems to differ from this. Observations of some AGN, GRB afterglows and PWNe have revealed an underlying 'hard' ($p < 2$) electron distribution (Panaitescu & Kumar 2001a; Shen, Kumar & Robinson 2006). Derivation of expressions for the radiation spectrum from such a distribution requires a different treatment from its 'soft' counterpart.

In this paper, we introduce a modelling platform for afterglow spectral evolution in the presence of a hard electron ($p < 2$) energy distribution. We then present the model of a few afterglows with such a hard spectrum, and derive their physical parameters.

★E-mail: resmi@iap.fr (LR); dipankar@iucaa.ernet.in (DB)

2 HARD ELECTRON ENERGY SPECTRUM

The distribution described in equation (1) can be safely assumed to go to infinity if it is soft, since the role of the higher energy end is negligible in total number and energy content of the distribution. Hence, the equations which form the basics of the standard afterglow modelling paradigm contain only γ_m and p.

However, a hard electron distribution can not be extended up to infinity, and requires to be terminated with an upper cut-off to keep the total energy from diverging. This upper cut-off, $\gamma_{\rm u}$, which is determined by the acceleration mechanism, plays a crucial role in the analytical treatment of $p < 2$ spectra. Since electrons towards the higher energy end dominate in the share of the total energy content in the distribution, the upper cut-off appears explicitly in the equations describing the spectral parameters. The distribution beyond $\gamma_{\rm u}$ could be a sharp drop, an exponential fall-off, or a steeper ($p > 2$) power law.

There have been previous studies to incorporate hard electron energy distributions in afterglow modelling. Bhattacharya (2001) (hereafter B01) has used $\gamma_{\rm u}$ which is a function of the bulk Lorentz factor (Γ) of the shock. The dependence on Γ is parametrized by an index q.

The time dependence of γ_m is altered by the introduction of $\gamma_{\rm u}$. This in turn modifies the spectral evolution. Moreover, a new break frequency corresponding to $\gamma_{\rm u}$ will appear in the spectrum.

Dai & Cheng (2001) (hereafter DC01) has followed the same approach but by constraining $\gamma_{\rm u}$ (in their notation, $\gamma_{\rm M}$) to be due to the termination of acceleration process by energy loss to synchrotron radiation. Their model is a special case of B01 with $q = -1/2$. This upper limit $\gamma_{\rm M}$, in typical conditions lie at very high energies.

Panaitescu & Kumar (2001b) (hereafter PK01) consider two conditions to determine the upper limit of the energy distribution. (i) The upper limit ($\gamma_{\rm M1}$) results when the acceleration time-scale becomes larger than the time-scale for radiative energy loss (same as DC01), and the corresponding break frequency lies much above the observation limit. (ii) In the second case, the distribution terminates at an upper cut-off ($\gamma_{\rm M2}$). A steeper power law is assumed beyond the cut-off. A constant fraction of the shock produced thermal energy is assumed to be contained in the electron distribution, the lower bound of the distribution γ_m is assumed to follow the same evolution as it does in the standard model. The evolution of $\gamma_{\rm M2}$ results from these two conditions. In the limit, $\gamma_{\rm M2} \gg \gamma_m$ and $\Gamma \gg 1$, $\gamma_{\rm M2}$ can be obtained analytically to be proportional to $\Gamma^{-\frac{p-1}{p-2}}$. The second assumption that γ_m follows its standard model behaviour is somewhat inappropriate in this context, since this behaviour corresponds to a condition where the effect of $\gamma_{\rm M2}$ is ignorable. In reality, $\gamma_{\rm M2}$ originates in some physical process which will have its own dependence on Γ, hence it is more appropriate to parametrize the evolution of $\gamma_{\rm M2}$ as a function of Γ.

In this paper, we continue the investigation of B01. The upper cut-off $\gamma_{\rm u}$ of B01 is identified as an injection break $\gamma_{\rm i}$, above which the electron distribution steepens to a power law with index $p_2 > 2$. We leave room for accommodating different processes, by keeping the parametrisation of $\gamma_{\rm i}$ to be that of B01. Our results differ from PK01 in having the evolution of γ_m and hence of the light curve, depending on the nature of the injection break. The flux decay index and the closure relations between the light curve decay slope and spectral slope also depend on the injection break, essentially the value of q, which is characteristic of the mechanism responsible for the upper cut-off.

3 MODIFIED ELECTRON DISTRIBUTION AND INJECTION BREAK

The *double slope* electron energy distribution with slopes p_1 and p_2 is represented as

$$N(\gamma_{\rm e}) = \begin{cases} K_{\rm e}\gamma_{\rm e}^{-p_1} & \gamma_m \leqslant \gamma_{\rm e} < \gamma_{\rm i}, \\ K'_{\rm e}\gamma_{\rm e}^{-p_2} & \gamma_{\rm i} \leqslant \gamma_{\rm e} < \infty. \end{cases} \tag{2}$$

Here, $K_{\rm e}$ is the normalization constant, which will depend on the number density of the ambient medium $n(r)$ and the bulk Lorentz factor Γ. $K'_{\rm e}$ can be written as $K_{\rm e}\gamma_{\rm i}^{(p_2-p_1)}$.

We modify the B01 parametrisation of $\gamma_{\rm i}$ to

$$\gamma_{\rm i} = \xi(\beta\Gamma)^q \qquad 1 \leqslant \gamma_{\rm i} \leqslant \infty \tag{3}$$

in order to accommodate the non-relativistic regime of expansion where $\Gamma \not\gg 1$ and $\beta \not\sim 1$. Using the standard result that the post-shock particle density and energy density are $4\Gamma n(r)$ and $4\Gamma(\Gamma-1)n(r)m_{\rm p}c^2$, respectively (Sari, Piran & Narayan 1998), one derives

$$K_{\rm e} = 4n(r)g_{\rm p}\,\frac{m_{\rm p}}{m_{\rm e}}\,\frac{\epsilon_{\rm e}}{\xi^{2-p_1}}\,\frac{1}{\beta^{q(2-p_1)}}\,[\Gamma-1]\,\Gamma^{[1-q(2-p_1)]}, \tag{4}$$

$$\gamma_m = \left[\frac{m_{\rm p}}{m_{\rm e}}\frac{\epsilon_{\rm e}}{\xi^{2-p_1}}f_{\rm p}\right]^{\frac{1}{(p_1-1)}}\,\left[\frac{1}{\beta^{q(2-p_1)}}\right]^{\frac{1}{(p_1-1)}}[\Gamma-1]^{\frac{1}{p_1-1}}\,\Gamma^{-\frac{q(2-p_1)}{p_1-1}}, \tag{5}$$

where, $m_{\rm p}$ and $m_{\rm e}$ are the proton and electron rest mass, respectively. The function $g_{\rm p} = f_{\rm p}(p_1-1)$ and $f_{\rm p} = \frac{(2-p_1)(p_2-2)}{(p_1-1)(p_2-p_1)}$.

3.1 New spectral break

The standard afterglow model has four spectral parameters: the synchrotron peak frequency, ν_m, the cooling break or the synchrotron cooling frequency, $\nu_{\rm c}$, corresponding to the Lorentz factor beyond which the electrons cool rapidly, the flux $f_{\rm p}$ at the peak frequency (ν_m or $\nu_{\rm c}$), and the synchrotron self-absorption (SSA) frequency, ν_a, above which the fireball is optically thin. The radiation spectrum emerging from a double

slope electron distribution will exhibit an additional "injection break", corresponding to the Lorentz factor $\gamma_{\rm i}$. Using the standard expression for synchrotron frequency $\nu_{\rm syn}(\gamma)$ for an electron Lorentz factor γ, one obtains

$$\nu_{\rm i} = \frac{0.286}{1+z}\frac{e}{\pi m_{\rm e} c}\xi^{2q}\Gamma^{1+2q}\beta^{2q}B, \tag{6}$$

where B is the post-shock magnetic field density, e is the electron charge, c is the velocity of light and z is the redshift of the burst.

Above this frequency the spectral slope steepens to the value corresponding to p_2 from that of p_1.

4 SPECTRUM: THE SOURCE FUNCTION METHOD

Instead of the usual approach of writing flux $f_\nu \propto \nu^{-\delta}$, we use the synchrotron source function along with the optical depth to obtain the final flux. Therefore,

$$f_\nu = S_\nu[1-\exp(-\tau_\nu)], \tag{7}$$

where S_ν is the synchrotron source function, which has the following functional form:

$$S_\nu = \begin{cases} S_{\nu_{\rm p}}\left(\frac{\nu}{\nu_{\rm p}}\right)^2 & \nu < \nu_{\rm p}, \\ S_{\nu_{\rm p}}\left(\frac{\nu}{\nu_{\rm p}}\right)^{5/2} & \nu > \nu_{\rm p} \end{cases}, \tag{8}$$

where $S_{\nu_{\rm p}}$ is the source function at peak frequency $\nu_{\rm p}$. For slow cooling (i.e. $\nu_m < \nu_{\rm c}$), $\nu_{\rm p} = \nu_m$ and for fast cooling (i.e. $\nu_{\rm c} < \nu_m$), $\nu_{\rm p} = \nu_{\rm c}$. $S_{\nu_{\rm p}}$ can be calculated as $S_{\nu_{\rm p}} = f_{\rm p}\tau_{\nu_{\rm p}}$, where $f_{\rm p}$ is a normalization constant, that equals the fllux that would have been expected at $\nu_{\rm p}$ if self-absorption were absent.

The optical depth due to synchrotron process varies as $\nu^{-5/3}$ when ν is less than $\nu_{\rm p}$ and $\nu^{-(p+4)/2}$ otherwise. Normalizing the optical depth to be unity at $\nu = \nu_a$, $\tau_{\nu_{\rm p}}$, the optical depth at $\nu = \nu_{\rm p}$ can be written as $[\frac{\nu_{\rm p}}{\nu_a}]^{-5/3}$ when $\nu_a < \nu_{\rm p}$ and $[\frac{\nu_{\rm p}}{\nu_a}]^{-(p+4)/2}$ when $\nu_a > \nu_{\rm p}$. The value of p in the latter expression is 2 for the fast cooling regime if $\nu_{\rm c} < \nu < \nu_m$. p is replaced by p_1 (p_1+1) and p_2 (p_2+1) in the slow (fast) cooling regime below and above $\nu_{\rm i}$, respectively.

For a double slope electron energy spectrum undergoing slow cooling,

$$\tau_\nu = \tau_{\nu_m} \times \begin{cases} \left(\frac{\nu}{\nu_m}\right)^{-5/3} & \nu < \nu_m \\ \left(\frac{\nu}{\nu_m}\right)^{-(p_1+4)/2} & \nu_m < \nu < (\nu_{\rm c}, \nu_{\rm i}) \\ \left(\frac{\nu_{\rm c}}{\nu_m}\right)^{-(p_1+4)/2}\left(\frac{\nu}{\nu_{\rm c}}\right)^{-(p_1+5)/2} & \nu_m < \nu_{\rm c} < \nu < \nu_{\rm i} \\ \left(\frac{\nu_{\rm i}}{\nu_m}\right)^{-(p_1+4)/2}\left(\frac{\nu}{\nu_{\rm i}}\right)^{-(p_2+4)/2} & \nu_m < \nu_{\rm i} < \nu < \nu_{\rm c} \\ \nu_m^{(p_1+4)/2}\,\nu_{\rm c}^{1/2}\,\nu_{\rm i}^{(p_2-p_1)/2}\,\nu^{-(p_2+5)/2} & (\nu_{\rm i}, \nu_{\rm c}) < \nu \end{cases}. \tag{9}$$

For fast cooling,

$$\tau_\nu = \tau_{\nu_{\rm c}} \times \begin{cases} \left(\frac{\nu}{\nu_{\rm c}}\right)^{-5/3} & \nu < \nu_{\rm c} \\ \left(\frac{\nu}{\nu_{\rm c}}\right)^{-3} & \nu_{\rm c} < \nu < \nu_m \\ \left(\frac{\nu_m}{\nu_{\rm c}}\right)^{-3}\left(\frac{\nu}{\nu_m}\right)^{-(p_1+5)/2} & \nu_{\rm c} < \nu_m < \nu < \nu_{\rm i} \\ \left(\frac{\nu_m}{\nu_{\rm c}}\right)^{-3}\left(\frac{\nu_{\rm i}}{\nu_m}\right)^{-(p_1+5)/2}\left(\frac{\nu}{\nu_{\rm i}}\right)^{-(p_2+5)/2} & \nu_{\rm c} < \nu_m < \nu_{\rm i} < \nu \end{cases}. \tag{10}$$

These expressions, along with equation (8), are substituted in equation (7) to obtain the final flux, which at a given time, is a function of the five spectral parameters (ν_m, ν_a, $\nu_{\rm c}$, $\nu_{\rm i}$ and $f_{\rm p}$).

To estimate these parameters, we first evaluate $\Gamma(r)$ and $r(t)$. For that, we use the expressions given by Huang et al. (2000), after correcting for redshift, which accommodates a smooth transition from an initial ultra-relativistic to the final non-relativistic regime of the fireball. Time-evolution of the half-opening angle (θ_j) depends on the lateral velocity of the jet in its comoving frame, which essentially is the sound velocity of the post-shock medium. The half-opening angle varies as $\frac{{\rm d}\theta_j}{{\rm d}r} = \frac{1}{\beta\Gamma}[\frac{c_{\rm s}}{c}]$, where $c_{\rm s}$ is the velocity of sound in the downstream medium. $c_{\rm s}$ is usually assumed to be constant throughout the evolution of the shock, but this is not a very accurate assumption. Initially, when the downstream plasma is ultra-relativistic, the thermal velocity will be $c/\sqrt{3}$, but as the ejecta becomes non-relativistic, the velocity approaches $\sqrt{\frac{k_{\rm B}T}{m_{\rm p}}}$, where $m_{\rm p}$ is rest mass of the proton. We calculate $c_{\rm s}$ as a function of Γ, adopting the method followed by Chandrasekhar (1939). This gives us

$$\left[\frac{c_{\rm s}}{c}\right]^2 = \frac{k_{\rm B}T}{m_{\rm p}c^2}\frac{1}{\Gamma}. \tag{11}$$

We have used equation (A3) (Appendix A) to obtain temperature in terms of Γ. More details of the calculation is given in Appendix A. The comoving magnetic field density B is given as $[8\pi\epsilon_{\rm B}\frac{(\Gamma-1)m}{V_{\rm co}}]^{\frac{1}{2}}c$, where $\epsilon_{\rm B}$ is the fraction of thermal energy in the magnetic field, m is the total swept up mass, $V_{\rm co}$ is the volume of the downstream plasma in the comoving frame, which can be calculated as $\Omega r^2\Delta'$, where Ω is the solid angle and Δ' is the comoving shell thickness.

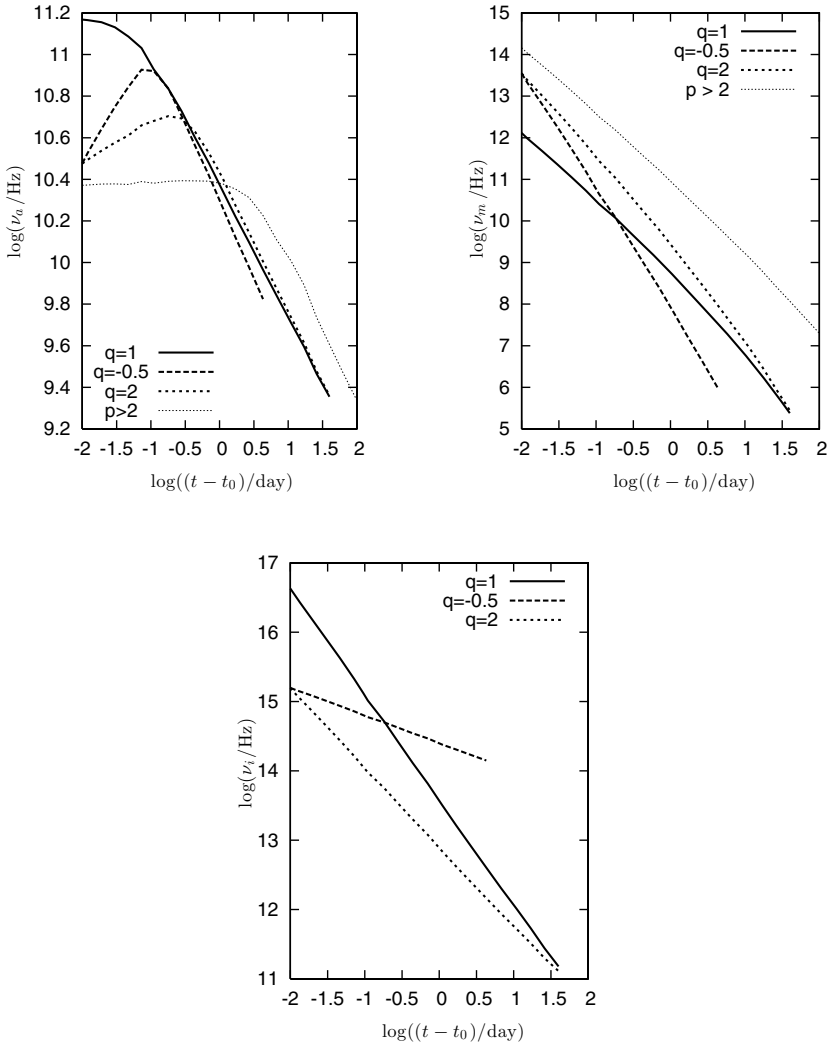

Figure 1. Evolution of spectral breaks ν_a (top left-hand panel), ν_m (top right-hand panel) and $\nu_{\rm i}$ (bottom) for different values of q. For comparison, result of a single power law with $p = 2.2$ is also shown (thin line). $\nu_{\rm i}$ is not relevant for the $p > 2$ case, however. The parameters used in calculating the curves are: $z = 1$, a spherical outflow of isotropic equivalent energy 10^{51} erg and initial Lorentz factor 350 in a homogeneous ambient medium of density 0.1 atom/cc. The shock microphysics parameters are: $\epsilon_{\rm e} = 0.1$, $\epsilon_{\rm B} = 0.01$, $p_1 = 1.5$, $p_2 = 2.2$ and $\xi = 2000$.

We calculate $f_{\rm p}$ using the expression (equation 25) given by Wijers & Galama (1999). ν_m and $\nu_{\rm c}$ are calculated using the expression described in Section 3.1, by replacing $\gamma_{\rm i}$ with γ_m (equation 5) and $\gamma_{\rm c} (= 6\pi m_{\rm e} c/(\sigma_{\rm T}\Gamma B^2 t))$. ν_a is the frequency at which the synchrotron optical depth in the comoving frame ($\alpha'_{\nu'}\Delta'$, where α_ν is the absorption coefficient calculated following the method given by Rybicki & Lightman 1979) equals unity.

For various values of q, the evolution of the spectral breaks as a function of time is plotted in Fig. 1 and the light curves are displayed in Fig. 2. The difference of evolution introduced by q is apparent in these figures.

5 DYNAMICS: LIMITING CASES

To obtain the overall dynamics of the fireball, we adopt the method presented by Huang et al. (2000) which accommodates a smooth transition from the initial ultra-relativistic to the final non-relativistic phase.

However, analytical solutions for $\Gamma(r)$ are possible in extreme cases. The adiabatic ($\epsilon = 0$) ultra-relativistic regime ($\Gamma \gg 1$, $\beta \sim 1$) is encountered most commonly in afterglow observations. At late times, ($t > t_{\rm NR}$, the fireball becomes non-relativistic. This phase is the same as that of the well-studied supernova remnants.

5.1 Ultra-relativistic Limit

In this limit, the expressions for $\Gamma(r)$ and r(t) of Huang et al. (2000) can be approximated to $\sqrt{(3-s)E_0/(\Omega c^2)}\ (\rho_0 r_0^3)^{-1/2}\ (r/r_0)^{(s-3)/2}$ and $((4-s)(3-s)2ct\,E_0/((1+z)\Omega c^2\rho_0 r_0^s))^{\frac{1}{4-s}}$, respectively, where $\rho(r)$, the ambient medium mass density profile is parametrized as $\rho_0\,(r/r_0)^{-s}$.

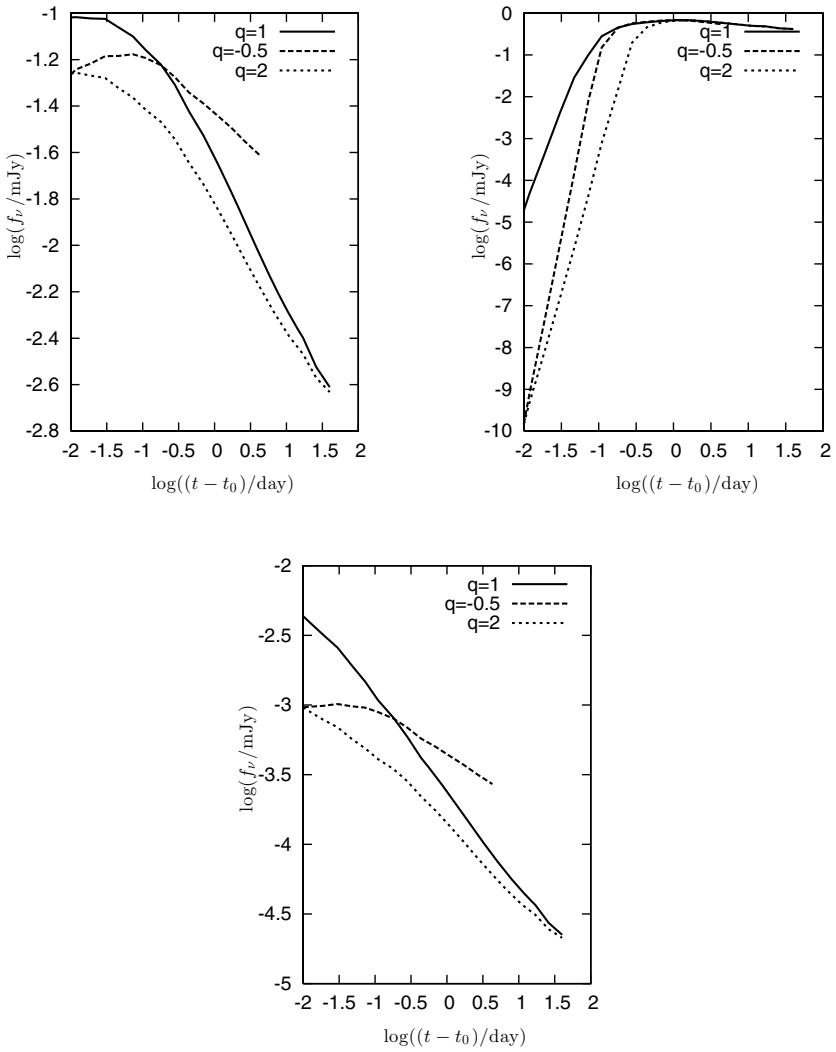

Figure 2. Left-hand top panel: sample model optical light curve (4×10^{14} Hz); right-hand top panel: X-ray light curve (10^{18} Hz) and (bottom) radio light curve for 22 GHz for three different values of q.

The expressions for spectral parameters we obtained for this phase, are listed below. We consider two types of ambient media: (i) a constant density around the progenitor star ($n(r) = n$, $s = 0$) and (ii) a stellar-wind blown stratified density profile ($s = 2$, with a normalization $\rho_0 = 5 \times 10^9\, A_\star$ and $r_0 = 10^{10}$ cm).

$$f_{\rm p}({\rm mJy}) = \begin{cases} 210.45\ \phi_{p_1}\ \frac{1+z}{d^2_{L,{\rm Gpc}}} \sqrt{\frac{\epsilon_{\rm s}}{c}}\ \sqrt{\epsilon_{\rm B}\, n}\ \mathcal{E}_{\rm iso,52} & (s=0) \\ 1021.5\ \frac{\phi_{p_1}(1+z)}{d^2_{L,{\rm Gpc}}} \sqrt{\mathcal{E}_{\rm iso,52}\epsilon_{\rm B}} A_\star \left[\frac{t_d}{(1+z)}\right]^{-1/2} & (s=2) \end{cases} \tag{12}$$

$$\nu_m({\rm Hz}) = \begin{cases} 1.87\times10^7\ (17.14)^{\frac{1-q(2-p_1)}{p_1-1}}\ \left[\frac{m_{\rm p}}{m_{\rm e}}\ f_{\rm p}\right]^{\frac{2}{p_1-1}}\ \sqrt{\frac{\epsilon_{\rm s}}{c}}\ \frac{x_{p_1}}{1+z}\ \sqrt{\epsilon_{\rm B} n}\ \epsilon_{\rm e}^{\frac{2}{p_1-1}} \\ \xi^{-2\frac{2-p_1}{p_1-1}}\ \left[\frac{\mathcal{E}_{\rm iso,52}}{n}\right]^{\frac{p_1+qp_1-2q}{4(p_1-1)}}\ \frac{t_d}{(1+z)}^{-\frac{3(p_1+qp_1-2q)}{4(p_1-1)}} & (s=0) \\ 5.77\times10^7\ (13.1)^y\ \sqrt{\frac{\epsilon_{\rm s}}{c}}\ \frac{x_{p_1}}{1+z}\ \left[\frac{m_{\rm p}}{m_{\rm e}} f_{p_1}\right]^{\frac{2}{p_1-1}}\ \mathcal{E}^{y/2}_{\rm iso,52}\ A_\star^{(1-y)/2} \\ \sqrt{\epsilon_{\rm B}}\ \epsilon_{\rm e}^{2/(p_1-1)}\ \xi^{\frac{-2}{(2-p_1)(p_1-1)}}\ \left[\frac{t_d}{(1+z)}\right]^{\frac{-(2+y)}{2}} & (s=2) \end{cases} \tag{13}$$

where $y = \frac{1-q(2-p_1)}{p_1-1}$, $\phi_{\rm p}$ and $x_{\rm p}$ are functions of p (Wijers & Galama 1999).

$$\nu_{\rm c}({\rm Hz}) = \begin{cases} 5.84\times10^{13}\ \left[\frac{\epsilon_{\rm s}}{c}\right]^3\ \mathcal{E}^{-1/2}_{\rm iso,52}\ n^{-1}\ \epsilon_{\rm B}^{-3/2}\ [t_d(1+z)]^{-1/2} & (s=0) \\ 7.6\times10^{11}\ \frac{1}{(1+z)^3}; \frac{\epsilon_{\rm s}}{c}^{-3/2}\ \epsilon_{\rm B}{}^{-3/2}\ A_\star^{-2}\ \mathcal{E}^{1/2}_{\rm iso,52}\ \left[\frac{t_d}{(1+z)}\right]^{1/2} & (s=2) \end{cases} \tag{14}$$

$$\nu_{\rm i}({\rm Hz}) = \begin{cases} 1.3\times10^{6}\ \frac{(4.14)^{1+2q}}{1+z}\ \sqrt{\frac{c_{\rm s}}{c}}\ \xi^{2}\ \sqrt{\epsilon_{\rm B}\,n}\ \left[\frac{\mathcal{E}_{\rm iso,52}}{n}\right]^{\frac{1}{4}(1+q)}\ \left[\frac{t_d}{(1+z)}\right]^{\frac{-3}{4}(1+q)} & (s=0) \\ 1.65\times10^{7}\ \xi^{2}(3.62)^{q}\sqrt{\frac{c_{\rm s}}{c}}\mathcal{E}_{\rm iso,52}^{q/2}A_{\star}^{(1+q)/2}\epsilon_{\rm B}^{1/2}\left[\frac{t_d}{(1+z)}\right]^{\frac{-1}{2}(2+q)} & (s=2) \end{cases}. \tag{15}$$

In the slow cooling regime,

$$\nu_{a}({\rm Hz}) = \begin{cases} (2.61\times10^{19})^{\frac{p_1}{4+p_1}}\ (8.38\times10^{19})^{\frac{2}{4+p_1}}\ (8.2\times10^{-7})^{\frac{2(p_1-1)}{4+p_1}}\ (0.88)^{\frac{2+p_1}{4+p_1}}\ (3)^{\frac{p_1+1}{p_1+4}} \\ (4.14)^{\frac{2(2-2q+p_1q)}{4+p_1}}\ (0.64)^{\frac{2+p_1}{4+p_1}}\ \left[\sqrt{\frac{c}{c_{\rm s}}}\right]^{\frac{p_1+2}{p_1+4}} \\ (2.3\times10^{-10})^{\frac{p_1}{p_1+4}}\left[\Gamma\left(\frac{3p_1+2}{12}\right)\ \Gamma\left(\frac{3p_1+22}{12}\right)\right]^{2/(p_1+4)}\ \left[1.87\times10^{-12}g_{\rm p}\sqrt{3}\frac{c_{\rm s}}{c}\right]^{\frac{2}{p_1+4}} \\ \mathcal{E}_{\rm iso,52}^{\frac{p_1+6+qp_1-2q}{4(p_1+4)}}\ \epsilon_{\rm B}^{\frac{p_1+2}{2(p_1+4)}}\ \epsilon_{\rm e}^{2/(p_1+4)}n^{\frac{p_1+6-qp_1+2q}{4(p_1+4)}}\ \xi^{-2\frac{2-p_1}{p_1+4}} \\ \left[\frac{t_d}{1+z}\right]^{\frac{-10-3p_1-3qp_1+6q}{4(p_1+4)}} & (s=0\ \ \nu_a<\nu_m) \\ \\ 2.61\times10^{14}\ \ (4.14)^{\frac{10q+3p_1-5qp_1-8}{5(p_1-1)}}\ \left[\frac{c_{\rm s}}{c}\right]^{23/40}\ \left[f_{\rm p}\frac{m_{\rm p}}{m_{\rm e}}\right]^{-\frac{3p_1+2}{5(p_1-1)}} \\ \left[\frac{(4-p_1^2)(p_2-2)}{(p_1+2/3)(p_2-p_1)}\right]^{3/5}\ \epsilon_{\rm B}^{1/5}\ \epsilon_{\rm e}^{\frac{-1}{(p_1-1)}}\xi^{\frac{2-p_1}{p_1-1}}\ \mathcal{E}_{\rm iso,52}^{\frac{18-13p_1-10q+5p_1q}{40(p_1-1)}}\ n^{\frac{14-19p_1+10q-5p_1q}{40(p_1-1)}} \\ \left[\frac{t_d}{1+z}\right]^{\frac{3(p_1-2)(q-1)}{8(p_1-1)}} & (s=0\ \ \nu_a<\nu_m) \end{cases} \tag{16}$$

Here, as well as in equations (17), (27) and (31), Γ denotes the gamma function and not the Bulk Lorentz factor of the shock.

$$\nu_{a}({\rm Hz}) = \begin{cases} (3.62)^{y_2}\ (3.42\times10^{53})^{\frac{1}{(p_1+4)}}\ (2.4\times10^{7})^{\frac{p_1}{(p_1+4)}}\ \left[g_{\rm p}\frac{\epsilon_{\rm e}}{\xi^{2-p_1}}\right]^{\frac{2}{(p_1+4)}} \\ \left[\sqrt{\frac{c_{\rm s}}{c}}\sqrt{\epsilon_{\rm B}}\right]^{\frac{p_1+2}{p_1+4}}\ \Gamma\left(\frac{3p_1+2}{12}\right)\ \Gamma\left(\frac{3p_1+22}{12}\right)\ \left[\frac{c_{\rm s}}{c}\right]^{\frac{2}{p_1+4}} \\ \mathcal{E}_{\rm iso,52}^{\frac{qp_1-2q}{2(p_1+4)}}\ A_{\star}^{\frac{1.+2p_1+4q-2p_1q}{p_1+4}}\ \left[\frac{t_d}{(1+z)}\right]^{\frac{2q-2p_1-qp_1-8}{2(p_1+4)}} & (s=2\ \ \nu_a>\nu_m) \\ 6.16\times10^{14}\ 3.62^{y_3}\ \left[\frac{p_1+2}{p_1+2/3}\right]^{3/2}\ \left[\frac{c_{\rm s}}{c}\right]^{23/40}\ \left[\frac{m_{\rm p}}{m_{\rm e}}f_{\rm p}\right]^{-\frac{2+3p_1}{5(p_1-1)}} \\ g_{\rm p}^{3/5}\epsilon_{\rm B}^{1/5}\ \mathcal{E}_{\rm iso,52}^{\frac{2}{5}+\frac{(p_1-2)(1-q)}{4(p_1-1)}}\ A_{\star}^{\frac{6}{5}-\frac{(p_1-2)(1-q)}{4(p_1-1)}}\ \left[\frac{\epsilon_{\rm e}}{\xi^{2-p_1}}\right]^{\frac{3}{5}-\frac{2+3p_1}{5(p_1-1)}} \\ \left[\frac{t_d}{(1+z)}\right]^{\frac{7p_1-2-10q+5p_1q}{20(p_1-1)}} & (s=2\ \ \nu_a<\nu_m) \end{cases} \tag{17}$$

where $y_2 = \frac{p_1+6-4q+2qp_1}{p_1+4}$ and $y_3 = \frac{(p_1-2)(1-q)}{p_1-1}$

In the fast cooling regime,

$$\nu_{a}({\rm Hz}) = \begin{cases} 1.96\times10^{11}\ (p_1-1)^{1/3}\ \left[\frac{c_{\rm s}}{c}\right]^{9/2}\ (1+z)^{2/3}\ \mathcal{E}_{\rm iso,52}^{1/6}\ n_0^{1/6}\ \left[\frac{t_d}{1+z}\right]^{-1/2} & \nu_{\rm c}<\nu_a<\nu_m\ \ (s=0) \\ 1.83\times10^{10}\ (p_1-1)^{3/5}\ \left[\frac{c_{\rm s}}{c}\right]^{57/10}\ (1+z)^{2}\ \mathcal{E}_{\rm iso,52}^{7/10}\ n_0^{11/10}\ \epsilon_{\rm B}^{6/5}\ \left[\frac{t_d}{1+z}\right]^{-1/2} & \nu_a<\nu_{\rm c}\ \ (s=0) \\ 1.44\times10^{9}\ (p_1-1)^{1/3}\ A_{\star}^{1/3}\ [t_d(1+z)]^{-2/3} & \nu_{\rm c}<\nu_a<\nu_m\ \ (s=2) \\ 8.48\times10^{7}\ (p_1-1)^{3/5}\ \left[\frac{c_{\rm s}}{c}\right]^{6/5}\ \mathcal{E}_{\rm iso,52}^{-2/5}\ A_{\star}^{11/5}\ \epsilon_{\rm B}^{6/5}\ \left[\frac{t_d}{1+z}\right]^{-8/5} & \nu_a<\nu_{\rm c}\ \ (s=2) \end{cases} \tag{18}$$

5.1.1 α–δ closure relations

The $\alpha-\delta$ closure relations for a general value of q valid in the slow cooling phase of the ultra-relativistic approximation are the following:

$$\alpha = \begin{cases} \frac{3}{8}\left[(q-1)-2\delta(q+1)\right] & \nu_m<\nu<\nu_{\rm c},\ \ t<t_j \\ \frac{1}{4}\left[(3q-1)-3\delta(q+1)\right] & \nu>\nu_{\rm c},\ \ t<t_j \\ \frac{1}{2}\left[q-3-2\delta(q+1)\right] & \nu_m<\nu<\nu_{\rm c},\ \ t>t_j \\ (q-1)-\delta(q+1) & \nu>\nu_{\rm c},\ \ t>t_j \end{cases}. \tag{19}$$

In Fig. 3, we display the above closure relations. The $q=1$ plot can be considered as a reference to the standard model, as it recovers the usual slopes. The dependence α has on q has to be kept in mind while inferring the value of p from the light curves. Temporal decay indices calculated for the ultra-relativistic limit are listed in Table 1 and light curve decay indices are listed in Table 2 (slow cooling) and in Table 3 (fast cooling).

5.2 Non-relativistic Limit

In the non-relativistic limit, at $t = t_{\rm NR}$, the Lorentz factor is $\sim$1 and $\beta \ll 1$. The fireball by this time would have undergone a considerable lateral spread and the geometry may be approximated to be spherical. The solid angle Ω may now be set to 4π.

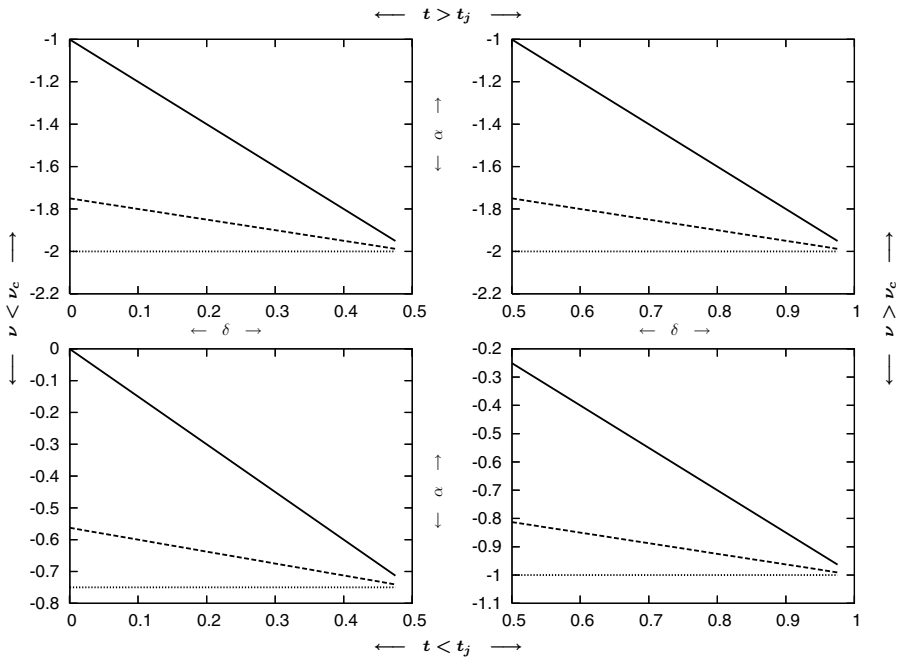

Figure 3. The $\alpha-\delta$ closure relations for various values of q. The left-hand panel shows the closure relations when the observing frequency is below the ν_c; the right-hand panel is for $\nu > \nu_c$. In the bottom panels, α is calculated before jet break. In the top panel, post-jet break α values are presented. The solid line is for $q = 1$, the dotted line is for $q = -0.5$ and the dashed line is for $q = -1$. For $q = 1$, the standard $p > 2$ scaling is recovered. Note that for $q = -0.5$, the minimum possible value of α is 1.75. For $q = -1$, α does not depend on δ.

Table 1. Temporal indices of the spectral parameters. For example, q and s.

Frequency	Before jet break	After jet break
ν_m	$\frac{s+(s-6)p_1-2q(2-p_1)(s-3)}{2(4-s)(p_1-1)}$	$\frac{2q-p_1-qp_1}{p_1-1}$
$\nu_a(\nu_a < \nu_m < \nu_c)$	$\frac{s(10q-4-p_1-5p_1q)+15(-p_1+p_1q-2q+2)}{10(4-s)(p_1-1)}$	$-\frac{7p_1-5p_1q+10q-12}{10(p_1-1)}$
$\nu_a(\nu_m < \nu_a < \nu_c)$	$\frac{s(2+p_1-4q+2p_1q)-6p_1-20+12q-6p_1q}{2(4-s)(p_1+4)}$	$\frac{(2q-4-p_1-qp_1)}{p_1+4}$
$\nu_a(\nu_a < \nu_c < \nu_m)$	$\frac{3}{5}+\frac{22}{5(s-4)}$	$-\frac{2}{3}$
$\nu_a(\nu_c < \nu_a < \nu_m)$	$\frac{6-s}{3(s-4)}$	$-\frac{6}{5}$
ν_i	$\frac{s(1+2q)-6(q+1)}{2(4-s)}$	$-(1+q)$
ν_c	$\frac{3s-4}{2(4-s)}$	0
f_{ν_m}	$-\frac{s}{2(4-s)}$	-1

5.2.1 Dynamics

The evolution of the radius r is calculated as

$$r = \zeta(\hat{\gamma}) \left[E_0 \frac{r_0^s}{\rho_0}\right]^{1/(5-s)} t^{2/(5-s)}, \tag{20}$$

where E_0 is the energy in the explosion and $\hat{\gamma}$ is the ratio of specific heats for the plasma. One could assume $\zeta(\hat{\gamma})$ to be 1.05 for a constant density ambient medium and 0.65 for a stellar-wind blown medium (Berger, Kulkarni & Frail 2004).

5.2.2 Electron energy spectrum

The thermal energy density in the shock downstream is estimated as

$$u_{\rm th} = \frac{9c^2\rho_0}{8}\,\beta^2\,\left(\frac{r}{r_0}\right)^{-s}, \tag{21}$$

where β is $\frac{1}{c}\frac{\mathrm{d}r}{\mathrm{d}t}$. The expressions for electron number and energy will give, respectively,

$$\frac{K_{\rm e}}{(p_1-1)\gamma_m^{p_1-1}} = 4\rho_0/m_{\rm p}\,\left(\frac{r}{r_0}\right)^{-s} \tag{22}$$

Table 2. The spectral indices (δ) and light curve decay indices (α_1; before jet break, α_2; after jet break) for various spectral regimes in slow cooling phase. Note that α depends upon the value q assumes. The expressions assume forms similar to those in $p > 2$ case, if q is set to unity.

Spectral segment	δ	α_1 (ISM,WIND)	α_2
$\nu < \nu_a < \nu_m < \nu_c$	2	$-\frac{(10-7p_1+3p_1q-6q)}{8(p_1-1)}$, $\frac{6-5p_1+p_1q-2q}{4(1-p_1)}$	$\frac{3p_1-6-3p_1q+6q}{6(p_1-1)}$
$\nu < \nu_m < \nu_a < \nu_c$			
$\nu_a < \nu < \nu_m < \nu_c$	$\frac{1}{3}$	$\frac{p_1+p_1q-2q}{4(P_1-1)}$, $\frac{2-p_1+p_1q-2q}{6(P_1-1)}$	$\frac{-2p_1+3-2q+qp_1}{3(p_1-1)}$
$\nu_m < \nu < \nu_a$	$\frac{5}{2}$	$\frac{5}{4}$, $\frac{7}{4}$	1
$\nu_m < \nu < \nu_i < \nu_c$	$-\frac{(p_1-1)}{2}$	$-\frac{3}{8}(p_1+p_1q-2q)$, $\frac{1}{4}(2q-p_1q-2p_1-1)$	$-\frac{2(q-1)-p_1(1+q)}{2}$
$\nu_m < \nu < \nu_c < \nu_i$			
$\nu_m < \nu_i < \nu < \nu_c$	$-\frac{(p_2-1)}{2}$	$-\frac{3}{8}(p_2+p_2q-2q)$, $\frac{1}{4}(2q-p_2q-2p_2-1)$	$-\frac{2(q-1)-p_2(1+q)}{2}$
$\nu_m < \nu_c < \nu < \nu_i$	$-\frac{p_1}{2}$	$\frac{1}{8}(6q-3p_1-3p_1q-2)$, $\frac{1}{4}(2q-p_1q-2p_1)$	$-\frac{2(q-1)-p_1(q+1)}{2}$
$\nu_m < \nu_i < \nu_c < \nu$	$-\frac{p_2}{2}$	$\frac{1}{8}(6q-3p_2-3p_2q-2)$, $\frac{1}{4}(2q-2p_2-p_2q)$	$-\frac{2(q-1)-p_2(q+1)}{2}$
$\nu_m < \nu_c < \nu_i < \nu$			

Table 3. Same as Table 2, but for fast cooling phase. After ν goes above both ν_c and ν_m, the respective positioning of these frequencies does not affect light curve slope and the indices will be the same as that of the corresponding slow cooling regime.

spectral segment	δ	α_1 (ISM,WIND)	α_2
$\nu < \nu_a < \nu_c$)	2	1, 2	1/9
$\nu_a < \nu < \nu_c$)	1/3	1/6, −2/3	−1
$\nu < \nu_c < \nu_a$)	2	1, 2	13/5
$\nu_c < \nu < \nu_a$)	5/2	5/4, 7/4	13/5
$(\nu_a, \nu_c) < \nu < \nu_m$	−1/2	−1/4, −1/4	−1

and

$$\frac{K_e m_e}{g_p}\,\gamma_i^{(2-p_1)} = \frac{9c^2\rho_0}{2}\epsilon_e\,\beta^2\,\left(\frac{r}{r_0}\right)^{-s}. \tag{23}$$

Solving equations (23) and (22), one obtains the expressions for K_e and γ_m:

$$K_e = \frac{9}{2}g_p\frac{\rho_0}{m_e}\,\frac{\epsilon_e}{\xi^{2-p_1}}\,\left(\frac{r}{r_0}\right)^{-s}\,\beta^{2-q(2-p_1)}, \tag{24}$$

$$\gamma_m = \left[\frac{9}{8}f_p\frac{m_p}{m_e}\frac{\epsilon_e}{\xi^{2-p_1}}\right]^{1/(p_1-1)}\,\beta^{\frac{2-q(2-p_1)}{p_1-1}}. \tag{25}$$

5.2.3 Spectral parameters

The magnetic field energy density is assumed, as usual, to be a fraction ϵ_B times the thermal energy density, that is,

$$B = \sqrt{9\pi\epsilon_B\beta^2c^2\rho(r)}. \tag{26}$$

We calculate the four spectral breaks, ν_a, ν_m, ν_c and ν_i and the peak flux f_p from

$$f_p = \frac{2.94\times10^{-21}}{d_L^2\,a}\,0.053^{(p_1-1)}\,\Gamma\left(\tfrac{3p_1+2}{12}\right)\,\Gamma\left(\tfrac{3p_1+22}{12}\right)\,r^3\,\frac{K_e\,B}{\gamma_m^{p_1-1}}, \tag{27}$$

$$\nu_m = 2.8\times10^6\,\frac{x_p}{(1+z)}\,B\,\left[2065.7\,f_p\frac{\epsilon_e}{\xi^{(2-p_1)}}\right]^{2/(p_1-1)}\,\beta^{\frac{2[2-q(2-p_1)]}{(p_1-1)}}, \tag{28}$$

$$\nu_c = 4.81\times10^{23}\,\frac{1}{B^2}\left[\frac{t}{t_{NR}}\right]^{-2}\,\left[\frac{t_{NR}}{1+z}\right]^{-2}, \tag{29}$$

$$\nu_{\rm i} = 8.0 \times 10^5 \, \frac{1}{(1+z)} \, B\xi^2\beta^{2q}, \tag{30}$$

$$\nu_a = \begin{cases} 4.72 \left[\frac{p_1+2}{p_1+2/3}\, K_{\rm e}\right]^{3/5} \gamma_m^{-(3p_1+2)/5} \; r^{3/5} B^{2/5} \quad (\text{for } \nu_a > \nu_m) \\ (6.72\times10^{-13})^{\frac{p_1-1}{p_1+4}} \, (1.25\times10^{19})^{\frac{p_1}{p_1+4}} \, (7\times10^{-5})^{\frac{1}{p_1+4}} \\ \left[\Gamma\left(\frac{3p_1+2}{12}\right)\, \Gamma\left(\frac{3p_1+22}{12}\right)\right]^{\frac{2}{p_1+4}} \; B^{\frac{p_1+2}{p_1+4}} \; \left[\frac{rK_{\rm e}}{a}\right]^{\frac{2}{p_1+4}} \quad (\text{for } \nu_a < \nu_m) \end{cases}, \tag{31}$$

where a is a numerical factor, describing the thickness of the shock in terms of r as $\Delta = r/a$

6 SYNCHROTRON SELF-COMPTON EMISSION

The contribution to the total flux from synchrotron photons which are Compton scattered by the non-thermal relativistic electrons themselves, can be significant towards higher energies.

We calculate this Compton component following the method adopted by Sari & Esin (2001). Following this work, the approximate ratio of inverse Compton (IC) to synchrotron luminosities may be estimated as follows (for a uniform density ambient medium and the slow cooling regime).

The IC spectrum is characterized by four break frequencies: $\nu_m^{\rm IC} = 2\gamma_m^2\nu_m^{\rm syn}$, $\nu_{\rm c}^{\rm IC} = 2\gamma_{\rm c}^2\nu_{\rm c}^{\rm syn}$, $\nu_{\rm i}^{\rm IC} = 2\gamma_{\rm i}^2\nu_{\rm i}^{\rm syn}$, $\nu_a^{\rm IC} = 2\gamma_m^2\nu_a^{\rm syn}$ and a flux normalization $f_{\rm p}^{\rm IC} = f_{\rm p}^{\rm syn}\sigma_{\rm T}\, n\, r$.

For $\nu_m^{\rm syn} \leqslant \nu_{\rm i}^{\rm syn} \leqslant \nu_{\rm c}^{\rm syn}$, the energy emitted by the Compton process peaks at $\nu_{\rm c}^{\rm IC}$ and that by the synchrotron process will peak at $\nu_{\rm c}^{\rm syn}$.

$$\begin{aligned} x \equiv \frac{L^{\rm IC}}{L^{\rm syn}} &\approx \frac{\nu_{\rm c}^{\rm IC}\, f_{\nu_{\rm c}}^{\rm IC}}{\nu_{\rm c}^{\rm syn}\, f_{\nu_{\rm c}}^{\rm syn}} \\ &= 700\mathcal{R}_{-7}\, \gamma_{c,7}^2 \left[\frac{\gamma_{m,500}}{\gamma_{i,5}}\right]^{(p_1-1)_{0.5}} \left[\frac{\gamma_{i,5}}{\gamma_{c,7}}\right]^{(p_2-1)_{1.5}}. \end{aligned} \tag{32}$$

For $\nu_m^{\rm syn} \leqslant \nu_{\rm c}^{\rm syn} \leqslant \nu_{\rm i}^{\rm syn}$, Compton energy peaks at $\nu_{\rm i}^{\rm IC}$ and synchrotron energy peaks at $\nu_{\rm i}^{\rm syn}$

$$\begin{aligned} x &\approx \frac{\nu_{\rm i}^{\rm IC}\, f_{\nu_{\rm i}}^{\rm IC}}{\nu_{\rm i}^{\rm syn}\, f_{\nu_{\rm i}}^{\rm syn}} \\ &\approx 700\mathcal{R}_{-7}\, \gamma_{i,7}\, \gamma_{c,5} \left[\frac{\gamma_{m,500}}{\gamma_{i,7}}\right]^{(p_1-1)_{0.5}}, \end{aligned} \tag{33}$$

where $\gamma_{e,n} = \gamma_{\rm e}/10^n$, $\gamma_{m,500} = \gamma_m/500$, $\mathcal{R}_{-7} = \frac{f_{\rm p}^{\rm IC}/f_{\rm p}^{\rm syn}}{10^{-7}}$ and $(p-1)_f = (p-1)/f$. In either case, the Compton power peaks at very high frequencies ($\sim 10^{21}$ Hz $\frac{B}{0.1{\rm G}}\frac{\Gamma}{100}$) for a hard electron spectrum. Hence, the contribution of synchrotron self-Compton emission becomes significant only at frequencies above hard X-rays.

As a next step, we estimate the IC flux from a numerical integration over the photon and the electron spectra. To do so we use the expression given by Sari & Esin (2001) for the IC flux due to the modified electron distribution, and the synchrotron radiation spectrum $f_\nu^{\rm syn}$ generated by this electron energy spectrum:

$$f_\nu^{\rm IC} = r\sigma_{\rm T} \int_{\gamma_m}^{\infty} {\rm d}\gamma \, N(\gamma) \int_0^{x_0} {\rm d}x f_\nu^{\rm syn}(x), \tag{34}$$

where $x_0 \sim 0.5$.

The synchrotron and the Compton fluxes obtained from the above calculation are displayed in Fig. 4.

7 MODELLING SHALLOW EVOLUTION

A new parameter q is required for modelling afterglow evolution based on hard electron energy spectrum. This index parametrizes the evolution of the upper cut-off of the electron spectrum (see equation 3). The value of q is determined by the acceleration process operating in the relativistic shocks. The present understanding about this from theoretical or numerical calculations is not exhaustive.

The termination of the acceleration process due to synchrotron radiation losses leads to $\gamma_{\rm i}$ being inversely proportional to the square-root of the bulk Lorentz factor ($q = -0.5$) (Gallant & Achterberg 1999; Li & Waxman 2006). However, the slowest post-jet break decay in this case tends to 1.75 as p_1 tends to its minimum possible value of 1 (in the limit $1 \leqslant p_1 \leqslant 2$). This is noticed by DC01 also, who have tried to model GRB010222 using a hard electron energy spectrum. They have used this fact to rule out the presence of a hard electron energy distribution in this afterglow. None of the afterglows we model in this paper, however, display post-jet break decays steeper than 1.75, which rules out the possibility of their electron distribution be terminated by synchrotron losses.

$q = 1$ is applicable to the lower cut-off of fermi process ($\gamma_{\rm i} = \frac{m_{\rm p}}{m_{\rm e}}\,\Gamma$), below which a pre-acceleration mechanism producing a flat electron spectrum may operate (Achterberg 2001). The presence of such an upper cut-off is observed in some of the AGN (Leahy, Muxlow & Stephens 1989; Konopelko et al. 2003; Stawarz et al. 2007) and PWNe (Hoshino et al. 1992). Moreover, $q = 1$ also provides scalings that would have

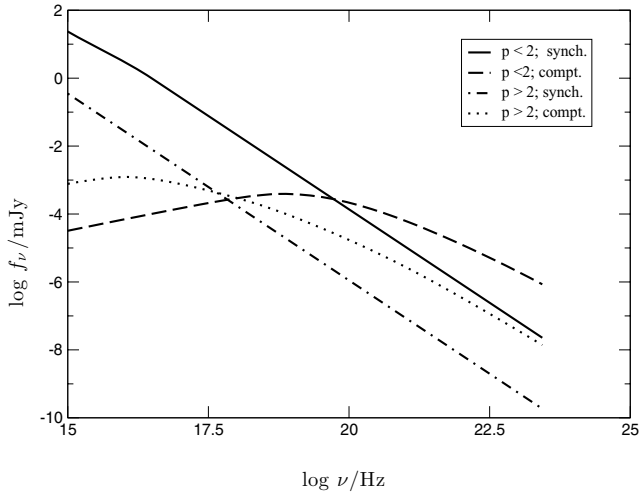

Figure 4. The predicted Compton contribution from hard electron energy spectrum, in comparison with that from a steep spectrum. For frequencies less than 10^{19} Hz, the contribution from SSA is rather low for $p < 2$ spectrum. The parameters used for calculation are, $\mathcal{E}_{\rm iso,52} = 10^2$, $n = 100$, $\epsilon_{\rm e} = 0.3$ and $\epsilon_{\rm B} = 10^{-3}$. For hard spectrum $p_1 = 1.8$, $p_2 = 2.2$, $q = 1$ and $\xi = 5000$ are used, and for steep spectrum a p of 2.2 is used. The displayed spectra are for ∼5 d post-burst.

been obtained in the standard fireball model without references to $\gamma_{\rm i}$. Good fits could be obtained with a q of 1 for all three afterglows we study (Bhattacharya & Resmi 2004; Misra et al. 2005); however, the value of ξ we inferred from these fits are far higher than $m_{\rm p}/m_{\rm e}$.

Another interesting value of q is -1.0, though any mechanism producing such an upper cut-off proportional to the inverse of the bulk Lorentz factor is not discussed in the literature to the best of our knowledge. $q = -1$ provides α_1 of 0.75 and α_2 of 2.0, independent of the value p assumes, as is obvious from equation (19) since δ is always multiplied by $(q + 1)$, which in this case vanishes. It is interesting that these α s correspond to $p > 2$ scaling relations if applied to a p of 2.

For GRB afterglows, it is not often very easy to infer the value of p unambiguously. The spectral index estimated from observations in the optical bands is a composite of the unknown host galaxy extinction and the intrinsic spectral index, δ. The X-ray spectrum is not affected by dust extinction but is modified by photoelectric absorption at lower energies. This makes the X-ray spectral index to be a function of the unknown gas column density along the line of sight. Also, due to the low count rate, it is often difficult to bin the spectrum and get the value of δ accurately. A third method is to measure the flux decay index past the jet break in optical and in X-ray wavelengths and assume it to be p, as predicted by the standard afterglow model. Though it suffers from complexities in the modelling of the fireball dynamics, this method is largely followed and trusted. However, the spectral index derived should be consistent with the closure relations between the temporal decay index, α and the spectral index, δ in various bands.

Recently several studies have suggested the possibility that the electron energy index, inferred by some of the above methods, falls below 2. Out of the 16 well-observed pre-*Swift* afterglows studied by Zeh, Klose & Kann (2006), α_2 of five afterglows fall below 2. Shen et al. (2006) along with blazars and PWNe, study a sample of well monitored X-ray afterglows observed by *BeppoSAX* and *Swift*. The inferred values of p fall below 2 for eight of them (see fig. 5 of Shen et al. (2006)). Early evolution of several X-ray afterglows monitored by *Swift* have shown an unprecedented 'flat' evolution (Nousek et al. 2006). Though not all of them may have an intrinsic flat electron energy spectrum (some could show shallow decay due to prolonged energy injection from the central engine), some are well within the expectations of hard spectrum models. In some of the *Swift* X-ray light curves (e.g. GRB050820, GRB051109A, GRB061024), the normal decay phase, which follows the shallow phase, has α values expected from an underlying hard electron energy spectrum (Liang et al. 2008).

In the following section, we model three pre-*Swift* afterglows, with rich multiband data set, showing evidence of an underlying hard electron energy spectrum. We consider q as a fit parameter and use a range of $-2. < q < +2$ while searching for the best fit.

7.1 GRB010222

GRB 010222 (Piro 2001), at a redshift of 1.477 (Jha et al. 2001; Mirabal et al. 2002), was one of the first afterglows seen with hard electron spectrum and it initiated theoretical work in that direction (B01; DC01).

The optical afterglow evolution was initially shallow ($\alpha_1 \sim 0.6$) and it steepened to an α_2 of 1.3–1.4 around ∼0.5 d (Sagar et al. 2001; Stanek et al. 2001). Around the same time the X-ray light curve also steepened from $\alpha_1 \sim 0.6$ to $\alpha_2 \sim 1.3$ (in't Zand et al. 2001). Assuming this early achromatic break to be due to the lateral expansion of the jet, a hard electron distribution is required to explain the evolution past this break. The spectral index, $\delta_{\rm o}$, within the optical band was found to be 0.89 ± 0.03 after correcting for Galactic extinction (Mirabal et al. 2002). The X-ray spectral index ($\delta_{\rm X}$) depends on the assumed value of neutral hydrogen column density of the host galaxy. (in't Zand et al. 2001; Björnsson et al. 2002); however, it falls in the range of 0.7–0.9.

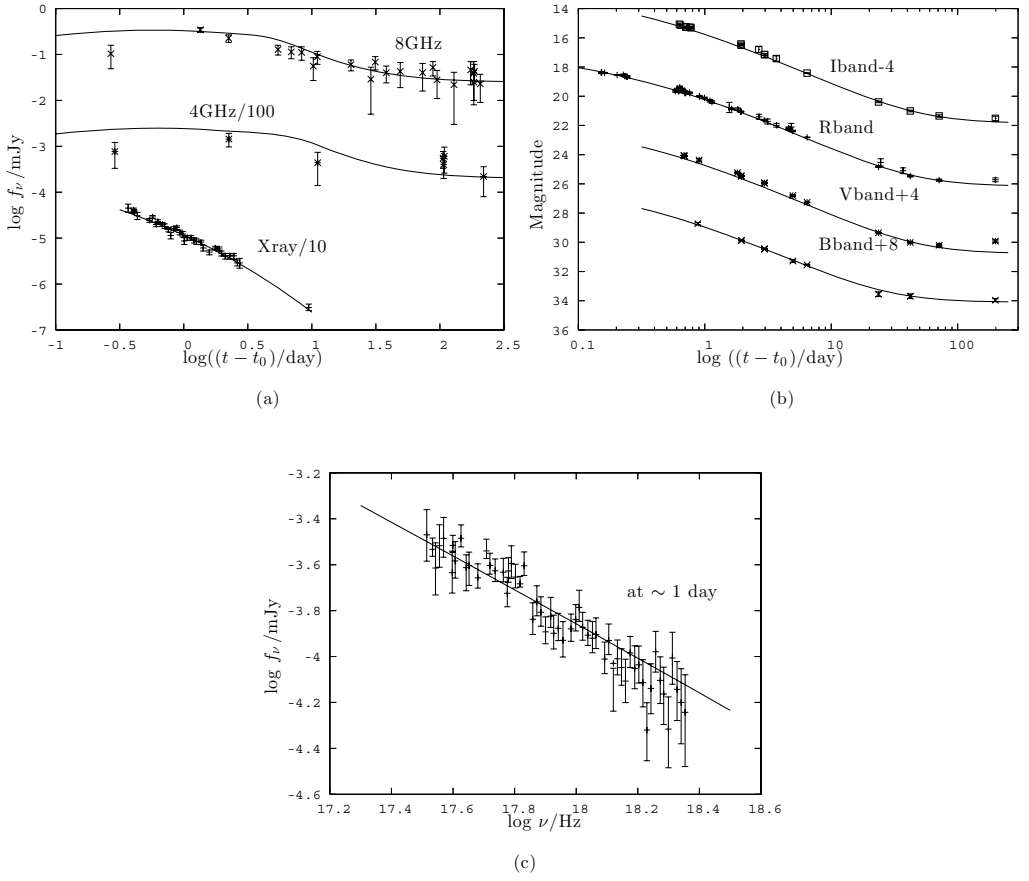

Figure 5. Multiband model fits for GRB010222. Points : observed data. Solid line : our model. (a) Radio and X-ray light curves. The 4 GHz light curve and the 10^{18} Hz X-ray light curve are offset by 0.01 and 0.1 mJy, respectively, for the ease of viewing. The flattening seen in radio light curves (panel a) are due to the flux of the starburst host SMM J14522+4301 (see text for details). (b) Optical *BVRI* light curves, appropriately offset to avoid clustering. (c) X-ray spectrum at $\sim$1 d from *BeppoSAX* along with the model.

Our model with $p_1 \sim 1.5$ and $q \sim 1.3$ reproduces the observed light curve decay indices before and after the jet break. We assume ν_c to be below both optical and X-ray bands at $\sim$0.5 d and ν_i to be above the X-ray bands. Along with the extinction in the host galaxy ($E(B-V) = 0.03$; starburst-type extinction law by Calzetti (1997)), this reproduces the observed optical and X-ray spectrum.

A model with q of 1.0 and ν_i in X-ray bands reproduces the data fairly well (Bhattacharya & Resmi 2004) and also explains the spectral steepening seen towards the X-ray band. (The X-ray spectral index derived by in't Zand et al. 2001 using the *Beppo-SAX* data is steeper than that in the optical bands.) However, our best fit is obtained when q is 1.3, not when it is unity. A higher q requires a steeper p_1 to reproduce the light curves decay indices as δ_1 and δ_2 decrease as q increases. The best fit with $q = 1.3$ (Fig. 5) requires that $\nu_i > \nu_X$.

We calculated the IC emission for these parameters, and found that it is negligible at the X-ray frequencies. We obtain a peak flux f_p of 1.04 mJy and the peak frequency ν_m of $\sim$200 GHz, at the time of the break. From these fit parameters, we infer an isotropic equivalent energy of $5.9 \times 10^{52} n_0^{1/5}$ erg, a jet opening angle of $2\overset{\circ}{.}1 n_0^{1/10}$, and a total energy of $3.6 \times 10^{49} n_0^{2/5}$ erg. An upper limit of 10^5 is estimated for ξ. The best-fitting model along with the observations are displayed in Fig. 5. The spectral parameters and physical parameters are listed in Tables 4 and 5, respectively.

We note that a model assuming continuous energy injection by Björnsson et al. (2002) can also reproduce the observed evolution of this afterglow. Another explanation for the achromatic break observed around $\sim$0.5 d is the non-relativistic transition of the fireball (Masetti et al. 2001), but such an early non-relativistic transition would require a very high ambient medium density ($n \sim 10^6$ atom/cc for the observed fluence of this burst) which would have suppressed the radio flux to nano-Jansky levels.

7.2 GRB020813

GRB020813 was detected by HETE-II (Villasenor et al. 2002) at a redshift of 1.26 (Price et al. 2002). The optical afterglow of this burst, like GRB010222, exhibited a shallow decay and an early break ($\alpha_1 \sim 0.8$, $t_b \sim 0.5$ d in optical, (Covino et al. 2003)). The X-ray observations started after the optical break, the light curve exhibited a single power-law decay consistent with the post-break optical decay ($\alpha_o \sim 1.4$ (Covino et al. 2003), $\alpha_X \sim 1.4$ (Butler et al. 2003)). The optical photometric spectral index, corrected for Galactic absorption was $\sim$0.9 (Covino et al. 2003) and the X-ray spectral index was $\sim$1.0 (Butler et al. 2003) with no absorption column in excess of the Galactic value of 7.5×10^{20} cm^{-2}.

Table 4. Fit parameters of the three modelled afterglows, given around the time of jet break.

Fit parameters	GRB010222	GRB020813	GRB041006
p_1	$1.47^{+0.004}_{-0.003}$	$1.40^{+0.007}_{-0.004}$	1.29–1.32
p_2	$2.04^{-0.01}_{+1.76}$	~ 2.1	>2.2
q	1.3 ± 0.06	1.3 ± 0.05	0.95–1.14
ν_m Hz	$2.24^{+9.4}_{-0.65} \times 10^{11}$	$3.99^{+1.58}_{-0.95} \times 10^{12}$	$(1.2–3.0) \times 10^{12}$
ν_c Hz	$9.03^{+0.37}_{0.36} \times 10^{13}$	$2.33^{+0.14}_{-0.28} \times 10^{13}$	$(1.0–2.0) \times 10^{14}$
ν_i Hz	$>10^{19}$	$>5 \times 10^{19}$	$>2.4 \times 10^{20}$
f_p mJy	$1.037^{+0.01}_{-0.108}$	$1.35^{+0.025}_{-0.065}$	(0.37–0.49)
t_j d	$0.56^{+0.035}_{-0.033}$	0.48 ± 0.03	0.17–0.24
$E\,(B-V)$ (host)	$0.035^{+0.005}_{-0.0035}$ mag	$0.03^{+0.006}_{-0.003}$ mag	0.01–0.05 mag
Host galaxy B band	$25.64^{+0.5}_{-0.25}$ mag	–	–
Host galaxy V band	$26.29^{+0.25}_{-0.5}$ mag	–	–
Host galaxy R band	$25.83^{+0.25}_{-0.3}$ mag	–	–
Host galaxy I band	25.59 ± 0.25 mag	–	–
Host galaxy 8.46 GHz	25^{+25}_{-19} μJy	–	–
Host galaxy 4.86 GHz	20^{+59}_{-10} μJy	–	–

Table 5. Derived physical parameters for the three afterglows. Since ν_a was not well constrained in all the cases, the parameters are presented as a function of the ambient density n_0, normalized to 1 atom/cc.

Physical parameters	GRB010222	GRB020813	GRB041006
$\epsilon_e\, n_0^{-\frac{p_1}{20}}$	$\sim$1.0	~ 1.0	~ 0.8
$\epsilon_B\, n_0^{\frac{3}{5}}$	$0.027^{+0.001}_{-0.002}$	$0.1^{+0.004}_{-0.007}$	0.07–0.14
$\xi\, n_0^{-\frac{1}{20}}$	$12.0^{+11.5}_{-3.9} \times 10^4$	$>5.7 \times 10^4$	$>2.0 \times 10^4$
$E_{\rm iso}\, n_0^{-\frac{1}{5}}$ erg	$5.83^{+0.14}_{-1.0} \times 10^{52}$	$3.22^{+0.076}_{-0.175} \times 10^{52}$	$(2.0–4.0) \times 10^{51}$
$\theta_j\, n_0^{-\frac{1}{10}}{}^\circ$	$2\overset{\circ}{.}0 \pm 0.008$	$2\overset{\circ}{.}3 \pm 0.05$	$1\overset{\circ}{.}7–2\overset{\circ}{.}8$
$E_{\rm tot}\, n_0^{-\frac{2}{5}}$ erg	$3.60 \pm 0.002 \times 10^{49}$	$2.2^{+0.4}_{-1.5} \times 10^{49}$	$(1.4–3.4) \times 10^{48}$

The value of p obtained from the best-fitting model is 1.4, for a q of 1.3. The jet break occurs at around half a day. We assumed ν_c to be $\sim 2.5 \times 10^{13}$ Hz at the time of the break, below the optical bands, to satisfy the observed α and δ in both X-ray and optical frequencies. The synchrotron peak frequency ν_m is around 4×10^{11} Hz at the time of the jet break and the peak flux f_{ν_m} is $\sim$1.4 mJy. The self-absorption frequency ν_a cannot be constrained using current observations. Our model requires additional extinction from the host, with rest frame A_V of 0.09 corresponding to an $E(B-V)$ of 0.04 and a starburst-type extinction law (Calzetti 1997).

The derived total energy of the burst is $3.6 \times 10^{49} n_0^{2/5}$ erg, confined in an opening angle of $2\overset{\circ}{.}3 n_0^{1/10}$. The upper limit on ξ is 10^4. The polarisation light curve of this afterglow has been explained in terms of a structured jet (Lazzati et al. 2004). The light curve from a structured jet viewed at an angle θ_0 hardly differs from that of a homogeneous jet with half-opening angle θ_0 (Rossi, Lazzati & Rees 2002) (especially for a jet structure described by a θ^{-2} power law). Hence, we can still safely assume the shallow power-law model for the electron energy distribution within the jet, even though we are not using the structured jet calculations. However, the total energy calculations will be affected, if the energy distribution is not homogeneous within the jet. If we assume that our inferred value of θ_0, which according to Rossi et al. will be the viewing angle, is approximately equal to the half-opening angle of the core of the structured-jet (Rossi et al. 2002), and if the actual extent of the jet is 90°, the energy inferred will be $\sim$9 times smaller than the true energy (see Rossi et al. for details).

The best-fitting model along with the observations is displayed in Fig. 6. The spectral parameters and physical parameters are listed in Tables 4 and 5, respectively.

7.3 GRB041006

We have presented multiband modelling of this afterglow, which is yet another example of a $p < 2$ electron distribution, in another paper (Misra et al. 2005). We therefore do not describe this in detail here. We assume the cooling frequency (ν_c) to be below the optical bands to satisfy α of 0.5 and δ in the range of 0.6–0.7 simultaneously. There is no signature of steepening seen at the higher energy end of the spectrum

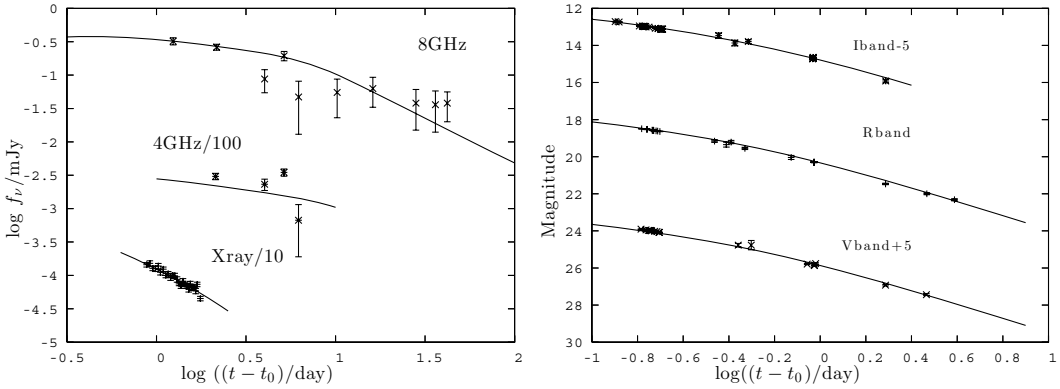

Figure 6. GRB020813: best-fitting model along with the observations. (i) The top two curves in the left-hand side panel are radio flux in 8.46 and 4.86 GHz, respectively. For ease of viewing, 4.86-GHz flux is multiplied by 0.01 mJy. The late time flattening in the 8-GHz data is not due to the presence of any host. Such flattening is seen in the radio afterglows beyond a few days past the burst, and is suspected to be some non-standard behaviour (see Frail et al. 2004) which is not taken care of by our code. The bottom curve in this panel is the X-ray light curve at 1.2×10^{18} Hz. (ii) The right-hand panel displays multiband optical light curves. *I* band is offset by -5 mag while *V* band is offset by $+5$ mag.

from the available observations. Hence, we place $\nu_{\rm i}$ above the X-ray band. We compute the spectral evolution of the afterglow with these basic assumptions. For the sake of completeness, we list the spectral and physical parameters from our model in Tables 4 and 5.

8 CONCLUSIONS

In GRB afterglows, as in other non-thermal sources, the shock accelerated electron spectrum at times assume a hard distribution (Leahy et al. 1989; Hoshino et al. 1992). However, almost all of the theoretical and modelling work in GRB afterglow physics, by default, assume a single steep power law for the distribution of electrons in the downstream plasma. The presence of a $p < 2$ spectrum, in a minority of cases, has, however, not received a fair share of attention. Calculations to derive the physical parameters of the burst in such cases are often not done consistently. Early attempts to model GRB afterglows with hard electron energy spectrum had several loopholes.

We have, in this paper, followed the approach of parametrising the temporal evolution of $\gamma_{\rm i}$ (thereby leaving room to account for different possible physical processes that could determine $\gamma_{\rm i}$) as $\gamma_{\rm i} \propto \Gamma^q$ (B01) and obtaining the afterglow flux decay index for different values of q. We have obtained expressions to calculate the observables from the physical parameters of the system which in turn can be used to derive the latter. We present multiband modelling of three afterglows, assuming ultra-relativistic expansion, and estimated their physical parameters.

For all these afterglows, we obtain good fits when $q \geqslant 1$. The inferred lower limit of ξ is around 10^4. Within the present understanding of particle acceleration physics, a mechanism which produces $q \geqslant 1$ and $\xi \sim 10^4$ is not known. However, future observations of GRB afterglows in the high energy range which can be achieved by upcoming satellites *GLAST* and *ASTROSAT* will shed more light on these parameters. For none of the three afterglows, the SSA frequency was well constrained. This left us with four observables and five unknowns, so we obtained the physical parameters as a function of the assumed value of ambient medium density. Though all of these afterglows were bright in their γ-ray output with isotropic equivalent energy in γ-rays $\sim 10^{52}$–10^{53} erg, the total kinetic energy derived from multiband modelling is relatively low ($\sim 10^{49}$ erg). This is partly due to the narrow beaming angle derived from an early jet break (for all the jets, θ is roughly $2\overset{\circ}{.}5$). Perhaps kinetic energy being an order of magnitude less than the energy output in radiation could be a trait associated with the presence of hard electron energy spectrum. More afterglows and their detailed modelling is required to examine this possibility. Another significant characteristic of all the three afterglows is a relatively low value of the synchrotron cooling frequency. While for most afterglows discussed in the literature, $\nu_{\rm c}$ remains above optical bands longer than a day after the burst, the three afterglows discussed here have, in our model, $\nu_{\rm c}$ falling below the optical band within 3 h.

The origin of the hard electron distribution is not yet clear. Different physical processes such as DSA (Achterberg et al. 2001), cyclotron wave resonance (Hoshino et al. 1992) etc. are beginning to be explored in detail in the context of relativistic shocks. Simulations of Fermi process in relativistic shocks including large angle scattering have resulted in hard electron energy spectra (Stecker, Baring & Summerlin 2007). Further developments in this area will hold the key to understanding the origin of the observed spectra of GRBs and their afterglows.

REFERENCES

Achterberg A., 2001, in Aharonian F. A., Völk H. J., eds, AIP Conf. Ser. Vol. 558, Particle Acceleration at Relativistic Shocks. Am. Inst. Phys., New York, p. 392

Achterberg A., Gallant Y. A., Kirk J. G., Guthmann A. W., 2001, MNRAS, 328, 393

Berger E., Kulkarni S. R., Frail D. A., 2004, ApJ, 612, 966

Bhattacharya D., 2001, Bull. Astron. Soc. India, 29, 107 (B01)

Bhattacharya D., Resmi L., 2004, in Feroci M., Frontera F., Masetti N., Piro L., eds, ASP Conf. Ser. Vol. 312, Evolution of an Afterglow with a Hard Electron Spectrum. Astron. Soc. Pac., San Francisco, p. 411

Björnsson G., Hjorth J., Pedersen K., Fynbo J. U., 2002, ApJ, 579, L59
Butler N. R., Marshall H. L., Ricker G. R., Vanderspek R. K., Ford P. G., Crew G. B., Lamb D. Q., Jernigan J. G., 2003, ApJ, 597, 1010
Calzetti D., 1997, AJ, 113, 162
Chandrasekhar S., 1939, An Introduction to the Study of Stellar Structure. Univ. Chicago Press, Chicago
Covino S. et al., 2003, A&A, 404, L5
Dai Z. G., Cheng K. S., 2001, ApJ, 558, L109 (DC01)
Ellison D. C., Double G. P., 2004, Astropart. Phys., 22, 323
Fermi E., 1949, Phys. Rev., 75, 1169
Frail D. A., Metzger B. D., Berger E., Kulkarni S. R., Yost S. A., 2004, ApJ, 600, 828
Gallant Y. A., Achterberg A., 1999, MNRAS, 305, L6
Hoshino M., Arons J., Gallant Y. A., Langdon A. B., 1992, ApJ, 390, 454
Huang Y. F., Gou L. J., Dai Z. G., Lu T., 2000, ApJ, 543, 90
in't Zand J. J. M. et al., 2001, ApJ, 559, 710
Jha S. et al., 2001, ApJ, 554, L155
Keshet U., 2006, Phys. Rev. Lett., 97, 221104
Konopelko A., Mastichiadis A., Kirk J., de Jager O. C., Stecker F. W., 2003, ApJ, 597, 851
Lazzati D. et al., 2004, A&A, 422, 121
Leahy J. P., Muxlow T. W. B., Stephens P. W., 1989, MNRAS, 239, 401
Li Z., Waxman E., 2006, ApJ, 651, 328
Liang E.-W., Racusin J. L., Zhang B., Zhang B.-B., Burrows D. N., 2008, ApJ, 675, 528
Masetti N. et al., 2001, A&A, 374, 382
Mirabal N. et al., 2002, ApJ, 578, 818
Misra K., Resmi L., Pandey S. B., Bhattacharya D., Sagar R., 2005, Bull. Astron. Soc. India, 33, 487
Nishikawa K.-I., Hededal C. B., Hardee P. E., Fishman G. J., Kouveliotou C., Mizuno Y., 2007, Ap&SS, 307, 319
Nousek J. A. et al., 2006, ApJ, 642, 389
Ostrowski M., Bednarz J., 2002, A&A, 394, 1141
Panaitescu A., Kumar P., 2001a, ApJ, 560, L49
Panaitescu A., Kumar P., 2001b, ApJ, 554, 667 (PK01)
Piro L., 2001, GRB Coordinates Network, 959, 1
Price P. A., Bloom J. S., Goodrich R. W., Barth A. J., Cohen M. H., Fox D. W., 2002, GRB Coordinates Network, 1475, 1
Rossi E., Lazzati D., Rees M. J., 2002, MNRAS, 332, 945
Rybicki G. B., Lightman A. P., 1979, Radiative Processes in Astrophysics. Wiley-Interscience, New York, p. 393
Sagar R. et al., 2001, Bull. Astron. Soc. India, 29, 91
Sari R., Esin A. A., 2001, ApJ, 548, 787
Sari R., Piran T., Narayan R., 1998, ApJ, 497, L17
Shen R., Kumar P., Robinson E. L., 2006, MNRAS, 371, 1441
Stanek K. Z. et al., 2001, ApJ, 563, 592
Stawarz Ł., Cheung C. C., Harris D. E., Ostrowski M., 2007, ApJ, 662, 213
Stecker F. W., Baring M. G., Summerlin E. J., 2007, ApJ, 667, L29
Villasenor J. et al., 2002, GRB Coordinates Network, 1471, 1
Wijers R. A. M. J., Galama T. J., 1999, ApJ, 523, 177
Zeh A., Klose S., Kann D. A., 2006, ApJ, 637, 889

APPENDIX A: CALCULATION OF THE LATERAL VELOCITY OF THE JET

The adiabatic sound velocity is defined as $c_s = \mathrm{d}P/\mathrm{d}\rho$ where P is the gas pressure and ρ is the mass density. Chandrasekhar (1939) derives the thermal energy density U_k of a monoatomic gas to be

$$U_k = n\left[\frac{3K_3(\Theta)+K_1(\Theta)}{4K_2(\Theta)} - 1\right] m_1c^2, \tag{A1}$$

where n is the particle number density in the gas and m_1 is mass of a single particle. $\Theta = m_1c^2/k_\mathrm{B}T$, where T is the temperature of the gas. $K_n(\Theta)$ is the modified Bessel function of order n. In terms of temperature, thermal energy density is usually expressed as $n\alpha(T)k_\mathrm{B}T$, where $\alpha(T)$ parametrizes the temperature dependence. It follows from the two expressions that

$$\alpha(T) = \Theta\left[\frac{3K_3(\Theta)+K_1(\Theta)}{4K_2(\Theta)} - 1\right]. \tag{A2}$$

In the non-relativistic regime, $\alpha(T)$ approaches the familiar value 3/2 and in the relativistic limit, it tends to 3. For a blast wave downstream plasma, with single particle rest mass m_1, the average thermal energy per particle $\alpha(T)k_\mathrm{B}T$ can be written as $(\Gamma - 1)m_1c^2$, that is,

$$m_1c^2\left[\frac{3K_3(\Theta)+K_1(\Theta)}{4K_2(\Theta)} - 1\right] = (\Gamma - 1)m_1c^2 \tag{A3}$$

from which we identify $[3K_3(\Theta) + K_1(\Theta)]/4K_2(\Theta)$ with Γ. Temperature of the gas can be solved for, in terms of Γ by inverting this relation.

However, the total energy density is independent of the dynamic regime of the gas and is given by, $u = \rho c^2 = (U_k + nm_1c^2)/V$ where ρ is the total (rest + inertial) mass density. Using this expression, we obtain

$$\frac{\rho}{P} = \Theta\frac{3K_3(\Theta)+K_1(\Theta)}{4K_2(\Theta)} = \Theta\Gamma, \tag{A4}$$

which gives the sound velocity in the downstream in terms of Γ as

$$\left[\frac{c_s}{c}\right]^2 = \frac{1}{\Theta\Gamma}. \tag{A5}$$

Let us examine the limiting values of the above expression and check the consistency. In the non-relativistic limit, $k_B\,T \ll m_1c^2$, that is, $\Theta \gg 1$, the Bessel function takes the form

$$K_n(\Theta) = \left[\frac{\pi}{2\Theta}\right]^{\frac{1}{2}} \exp(-\Theta)\left[1 + \frac{4n^2-1}{8\Theta}\right]. \tag{A6}$$

Substituting equation (A6) in equation (A5) we have

$$c_s^2 = \frac{k_B T}{m_1}\frac{4\left[1+\frac{15}{8\Theta}\right]}{3\left[1+\frac{35}{8\Theta}\right]+\left[1+\frac{3}{8\Theta}\right]}. \tag{A7}$$

Neglecting terms of the order of $1/\Theta$, expression for sound velocity in a non-relativistic gas is reduced to

$$c_s^2 = \frac{k_B T}{m_1}. \tag{A8}$$

Now, in the relativistic limit, that is, when $\Theta \ll 1$ the limiting expression for Bessel function is

$$K_n(\Theta) = \frac{1}{2}\frac{(n-1)!}{\left(\frac{\Theta}{n}\right)^n}. \tag{A9}$$

Substituting the above expression in equation (12), and neglecting terms $O(\Theta^2)$, we get for the sound velocity in a relativistic gas

$$c_s^2 = \frac{k_B T}{m_1}\frac{8\Theta}{24} = \frac{c^2}{3}. \tag{A10}$$

We calculate the the lateral velocity of matter in the fireball as it decelerates, using equation (A5). When $\Gamma \to 1$, we shift to the non-relativistic expression given by equation (A8).

This paper has been typeset from a TEX/LATEX file prepared by the author.